

Chiral Properties of Pseudoscalar Mesons on a Quenched 20^4 Lattice with Overlap Fermions

S.J. Dong^a, T. Draper^a, I. Horváth^a, F.X. Lee^{b,c}, K.F. Liu^a, and J.B. Zhang^d

^a*Dept. of Physics and Astronomy, University of Kentucky, Lexington, KY 40506*

^b*Center for Nuclear Studies, Dept. of Physics, George Washington University,
Washington, DC 20052*

^c*Jefferson Lab, 12000 Jefferson Avenue, Newport News, VA 23606*

^d*CSSM and Dept. of Physics and Math. Physics, University of Adelaide, Adelaide,
SA 5005, Australia*

Abstract

The chiral properties of the pseudoscalar mesons are studied numerically on a quenched 20^4 lattice with the overlap fermion. We elucidate the role of the zero modes in the meson propagators, particularly that of the pseudoscalar meson. The non-perturbative renormalization constant Z_A is determined from the axial Ward identity and is found to be almost independent of the quark mass for the range of quark masses we study; this implies that the $O(a^2)$ error is small. The pion decay constant, f_π , is calculated from which we determine the lattice spacing to be 0.148 fm. We look for quenched chiral log in the pseudoscalar decay constants and the pseudoscalar masses and we find clear evidence for its presence. The chiral log parameter δ is determined to be in the range 0.15 – 0.4 which is consistent with that predicted from quenched chiral perturbation theory.

PACS numbers: 11.15.Ha, 12.38.Gc, 11.30.Rd

1 Introduction

One of the main goals of lattice QCD is to understand from first principles low-energy phenomenology as a consequence of chiral symmetry. Recent advances in the formulation of chiral fermions on the lattice hold great promise for studying chiral symmetry of QCD at finite lattice spacing [1].

Neuberger's overlap fermion [2], derived from the overlap formalism [3], is such a chiral fermion on the lattice and has been implemented numerically to study the chiral condensate [4, 5, 6, 7], quark mass [8, 7], renormalization constants [8, 7, 9], and short-distance current correlators [10] and to check chiral symmetry [8, 11] and scaling [8]. However these studies are limited to small volumes due to the large numerical cost associated with approximating the matrix sign function. In this paper, we shall study physical observables, such as the pseudoscalar meson masses and pion decay constants, close to the physical u, d quark mass. As such, we need to work on a lattice which is at least 3 times larger than the Compton wavelength of the pion with the smallest mass in order to alleviate finite volume effects. We work on a 20^4 lattice with $a = 0.148$ fm as determined from the pion decay constant f_π . This gives the lattice size $La = 3.0$ fm and the smallest pion mass is ~ 280 MeV. Thus, the lattice size is ~ 4 times the Compton wavelength of the lowest-mass pion.

This paper is organized as follows. We will give the numerical details of the calculation in Sec. 2. In Sec. 3, we shall discuss the effect of the zero modes in the meson propagators. In view of the fact that the scalar condensate receives a contribution from the zero modes (which goes away in the infinite volume limit) through the generalized Gell-Mann-Oakes-Renner (GOR) relation, the pseudoscalar correlator should also be contaminated by the zero modes. We have observed the effect of the zero modes in the pseudoscalar propagator at small quark mass. After clarifying the zero mode issue, we proceed to calculate the non-perturbatively determined renormalization constant Z_A from the axial Ward identity and the pion decay constant f_π . We find that f_π is free of the quenched chiral log singularity and has a small error in the chiral limit. Thus, it is a good quantity to set the lattice scale. We present the results in Sec. 4. In Sec. 5, we explain our effort in searching for the predicted quenched chiral logs. We see the chiral logs in the pseudoscalar masses, the pseudoscalar matrix element f_P , and the f_P/f_π ratio at very small quark masses. A summary is given in Sec. 6.

2 Numerical Details

For Neuberger's overlap fermion [2], we adopt the following form for the massive Dirac operator [9, 12, 13]

$$D(m_0) = (1 - \frac{m_0 a}{2\rho})\rho D(\rho) + m_0 a, \quad (1)$$

where

$$D(\rho) = 1 + \gamma_5 \epsilon(H), \quad (2)$$

so that

$$D(m_0) = \rho + \frac{m_0 a}{2} + (\rho - \frac{m_0 a}{2})\gamma_5 \epsilon(H), \quad (3)$$

where $\epsilon(H) = H/\sqrt{H^2}$ is the matrix sign function and H is taken to be the hermitian Wilson-Dirac operator, i.e. $H = \gamma_5 D_w$. Here D_w is the usual Wilson fermion operator, except with a negative mass parameter $-\rho = 1/2\kappa - 4$ in which $\kappa_c < \kappa < 0.25$. We take $\kappa = 0.19$ in our calculation which corresponds to $\rho = 1.368$. The massive overlap action is so defined so that the tree-level renormalization of mass and wavefunction is unity. The bare mass parameter ^{*}, m_0 , is proportional to the quark mass without an additive constant which we have verified numerically in a previous study [8].

We adopt the optimal rational approximation [14, 8] to approximate the matrix sign function. The inversion of the quark matrix involves nested do loops in this approximation. It is found that it is cost effective to project out a relatively few eigenmodes with very small eigenvalues in the operator H^2 in order to reduce the condition number and speed up the convergence in the inner do loop [4, 8]. At the same time, this improves chiral symmetry relations such as the Gell-Mann-Oakes-Renner relation [8]. However, it is shown [15] that the density of these small eigenmodes grows as $e^{\sqrt{a}}$ with a being the lattice spacing. As a result, it is very costly and impractical to work on large volumes with the lattice spacings currently used. There are simply too many small eigenmodes to be projected out.

For this reason, we explore other options to clear this hurdle. We have tested the tree-level tadpole-improved Lüscher-Weisz gauge action [16] and find that the density of these small eigenvalue modes is decreased to a point where it becomes feasible to go to large volumes with a lattice size 4 times the Compton wavelength of the lightest pion. We further find that the anisotropic action [17] requires projection of more small eigenvalues in H^2 in order to achieve the same convergence in the inner loop than does the isotropic one. Thus, we decide to use the isotropic action. We also find that using the clover action with either sign requires the projection of more small eigenvalue modes. Therefore we use the Wilson action for H in the Neuberger operator. On a 20^4 lattice with $\beta = 7.60$ tree-level tadpole-improved Lüscher-Weisz gauge action, we project out 85 small eigenmodes. Beyond these eigenmodes, the

^{*}Note that we used a different normalization in the action before in [8]. As a result the bare mass here is equal to ρ times the bare mass in [8].

level density becomes large. As a result, the number of conjugate gradient steps is about 345 for the inner loop and about 300 for the outer loop. While the number for the inner do loop seems to be fairly independent of the lattice volume, the number for the outer do loop is about a factor of 2 larger than those for the Wilson gauge action on small volumes [8].

Since the conjugate gradient algorithm accommodates multiple masses with a minimum overhead, we calculated 16 quark masses ranging from $m_0a = 0.01505$ to $m_0a = 0.2736$ which are listed in Table 1 together with the number of configurations for each mass.

From the string tension with $\sqrt{\sigma} = 440$ MeV, we find that $a = 0.13$ fm. However, as we shall see later in Sec. 4, the scale determined from f_π is 0.148(2) fm which makes the physical length of the lattice to be 3.0 fm. The smallest pion mass turns out to be ~ 280 MeV so that the size of the lattice is ~ 4.1 times of the Compton wavelength of the lowest mass pion and more than 4 times for the heavier ones.

We adopt the periodic boundary condition for the spatial dimensions and the fixed boundary condition in the time direction so that we can have effectively a longer range of time separation between the source and sink to examine the meson propagators with small quark masses which lead to longer correlation lengths. The source of the meson interpolation field is placed at the 3rd time slice and we consider the sink as far as the 16th time slice to mitigate the boundary effect. This gives us a time separation of 13.

We have varied statistics for different quark masses. Of the 16 cases, 7 have 25 gauge configurations, one has 53, and the remaining 8 have 63 configurations. In order to carry out correlated fits to extrapolate observables to the physical pion mass, we construct the covariance matrix by embedding the one with smaller dimension, e.g. 25 and 53 into the one with dimension 63 in a block diagonal form. For example, the covariance C_{ij} for the one with 25 configurations is constructed so that $C_{ij}(i \leq 25, j > 25) = 0, C(i > 25, j \leq 25) = 0$ and $C_{ij}(i, j > 25) = \delta_{ij}$.

Table 1: Quark mass m_0a and number of gauge configurations are listed.

m_0a	0.01505	0.01642	0.01915	0.02736	0.04104	0.05472	0.06840	0.08208
# cfg.	25	25	63	63	53	63	25	63
m_0a	0.09576	0.1094	0.1368	0.1642	0.1915	0.2189	0.2462	0.2736
# cfg.	25	63	25	63	25	63	25	63

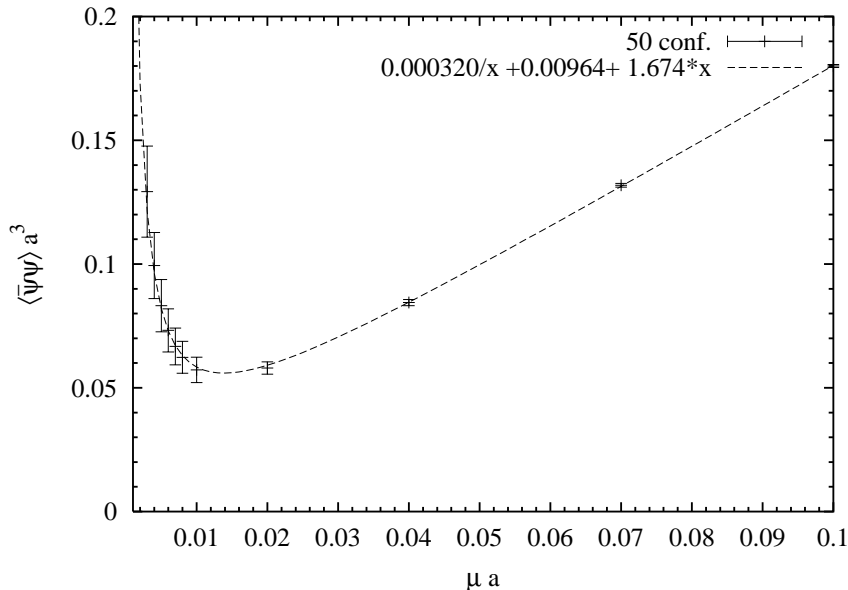


Figure 1: $\langle \bar{\psi}\psi \rangle$ as a function of the quark mass. We used 50 configurations of a $6^3 \times 12$ lattice with Wilson gauge action at $\beta = 5.7$. Here $\mu a = m_0 a / 2\rho$.

3 Zero Mode Effects in Meson Propagators

The quark zero mode is known to contribute to the vacuum scalar density $\langle \bar{\psi}\psi \rangle$ on a finite volume. The latter can be written in the following form for small quark mass m_0^\dagger

$$-\langle \bar{\psi}\psi \rangle = \frac{\langle |Q| \rangle}{m_0 V} + c_0 + c_1 m_0, \quad (4)$$

where Q is the topological charge which, according to the Atiya-Singer theorem, is the difference between the number of left-handed and right-handed zero modes (i.e. $Q = n_- - n_+$) and has been shown to hold for overlap fermions or other local fermion actions which satisfy the Ginsparg-Wilson relation [18, 19]. Since $\langle |Q| \rangle$ grows as \sqrt{V} , the zero mode contribution vanishes in the infinite volume limit while keeping m_0 fixed at a non-zero value. Thus the quark condensate which is the infinite volume and zero mass limit of $\langle \bar{\psi}\psi \rangle$ is represented by c_0 in Eq. (4). However, on a fixed finite volume lattice, this zero mode contribution is divergent for small enough m_0 . This was first observed in the domain-wall formulation [20] and is also seen in the overlap fermion [21]. Here we reproduce it in Fig. 1 which shows the divergent part of $\langle \bar{\psi}\psi \rangle$ from the zero modes for a $6^3 \times 12$ lattice with the Wilson gauge action at $\beta = 5.7$.

We see from Fig. 1 that c_0 is non-zero in this range of the quark mass and upon extrapolation to the infinite volume before taking the chiral limit defines the quark condensate $-\Sigma$. However, if one keeps volume fixed and lets the quark mass approach zero, e.g. $m_0 a < 0.001$, it is then found [4, 5, 21] that c_0 becomes zero. It is known [22] that when the size of the lattice is much smaller than the pion Compton wavelength,

[†]We shall address the quenched chiral log issue separately in Sec. 5.

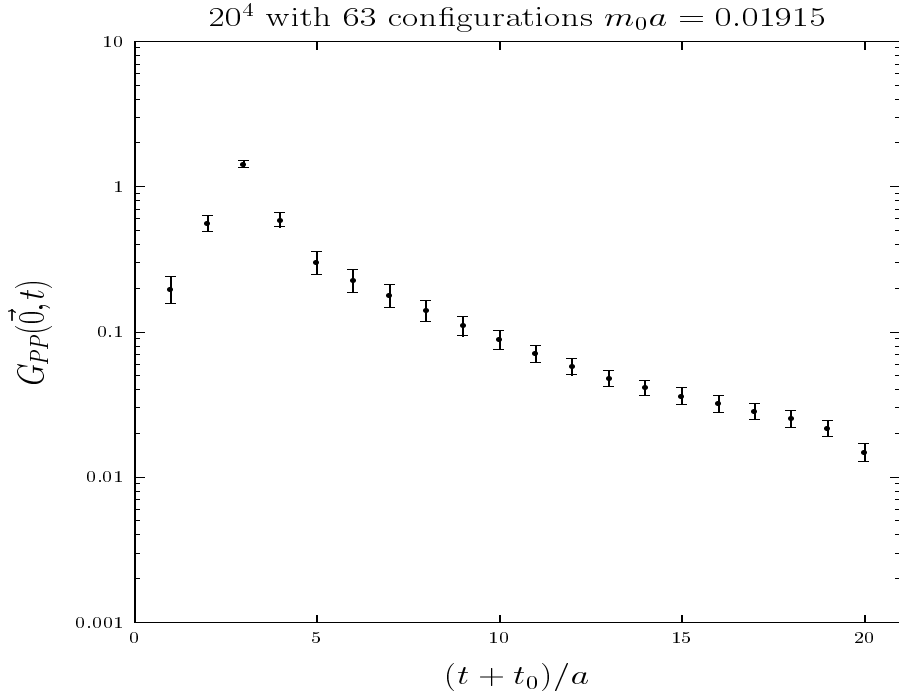


Figure 2: Pion propagator for $m_0a = 0.01915$ for all 63 configurations. The source is placed at $t_0/a = 3$

i.e. $L \ll 1/m_\pi$, the constant term vanishes and $\langle \bar{\psi}\psi \rangle$ is proportional to $m_0\Sigma^2V$ for small masses aside from the $\frac{\langle [Q] \rangle}{m_0V}$ term. Using finite size scaling, the chiral condensate Σ can be extracted [5].

While we have a reasonably good understanding of the role of zero modes in $\langle \bar{\psi}\psi \rangle$, their role in the hadron propagators is only beginning to be investigated in the domain-wall formalism [23] and the overlap formalism [6, 7] and its detailed influence on the hadron propagators is not fully understood. We shall investigate it in the pseudoscalar meson channel. There has been some concern about the behavior of the pion mass. It is not clear if it approaches zero in a finite volume in the chiral limit. In fact, one finds that the pion mass squared appears to approach a non-zero value on small lattices [24, 25]. To understand the situation, we first examine the generalized Gell-Mann-Oakes-Renner (GOR) relation

$$\frac{2(2m_0)^2}{V} \int d^4x d^4y \langle \pi^a(x) \pi^a(y) \rangle = -2m_0 \langle \bar{\psi}\psi \rangle. \quad (5)$$

The left hand side of Eq. (5) has a contribution of $\frac{2\langle [Q] \rangle}{V}$ as does the right hand side. Assuming the remainder of the pseudoscalar susceptibility is dominated by the pion, it is approximately $-f_\pi^2 m_\pi^2$. Comparing with Eq. (4), we get

$$f_\pi^2 m_\pi^2 = 2m_0 c_0 + 2m_0^2 c_1. \quad (6)$$

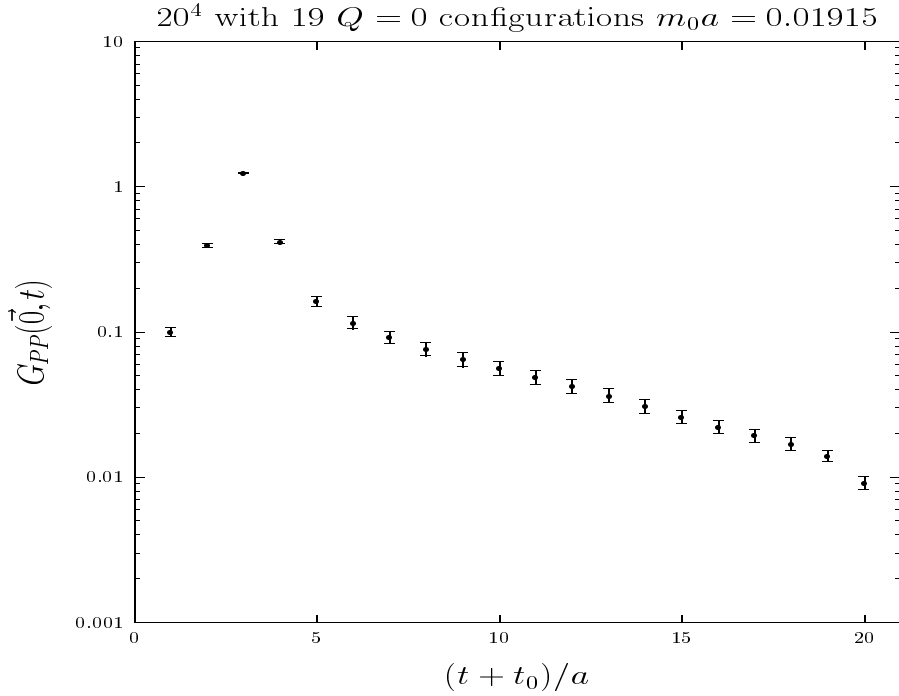


Figure 3: Pion propagator for $m_0 a = 0.01914$ for 19 configurations with $Q = 0$.

From this we see that m_π^2 approaches zero as m_0 for those volumes where c_0 is non-zero. On the other hand, when the m_0 is so small that c_0 becomes zero for certain fixed volume, the r.h.s. of Eq. (6) is survived by the next leading term with c_1 which is proportional to m_0^2 . As a result, one expects that m_π to be linearly proportional to m_0 . Here we have ignored the complication due to the quenched chiral log which we will address in Sec. 5.

Next, we turn to the zero-momentum pseudoscalar propagator $\int d^3x \langle \pi^a(x) \pi^a(0) \rangle$ which has two terms due to the zero modes as pointed out in the study of domain wall fermions [23]

$$\int d^3x \langle \pi(x) \pi(0) \rangle = \int d^3x \left[\sum_{i,j=\text{zero modes}} \frac{\text{tr}(\psi_j^\dagger(x) \psi_i(x)) \text{tr}(\psi_i^\dagger(0) \psi_j(0))}{m_0^2} + 2 \sum_{i=0, \lambda > 0} \frac{\text{tr}(\psi_\lambda^\dagger(x) \psi_i(x)) \text{tr}(\psi_i^\dagger(0) \psi_\lambda(0))}{m_0(\lambda^2 + m_0^2)} \right] + \frac{|\langle 0 | \pi(0) | \pi \rangle|^2 e^{-m_\pi t}}{2m_\pi}. \quad (7)$$

The first term is purely the zero-mode contribution. The second term is the cross term between the zero modes and the non-zero modes. We have used the property that the non-zero modes come in pairs which are related by γ_5 , i.e. $\gamma_5 \psi_\lambda = \psi_{-\lambda}$. Upon integrating the propagator with respect to time, we find

$$\int d^4x \langle \pi(x) \pi(0) \rangle = \frac{\sum_{i=0} \text{tr}(\psi_i^\dagger(0) \psi_i(0))}{m_0^2} + \frac{\sum_{i=0, \lambda > 0} \delta_{i\lambda} \text{tr}(\psi_i^\dagger(0) \psi_\lambda(0))}{m_0(\lambda^2 + m_0^2)} + \frac{|\langle 0 | \pi(0) | \pi \rangle|^2}{2m_\pi^2}. \quad (8)$$

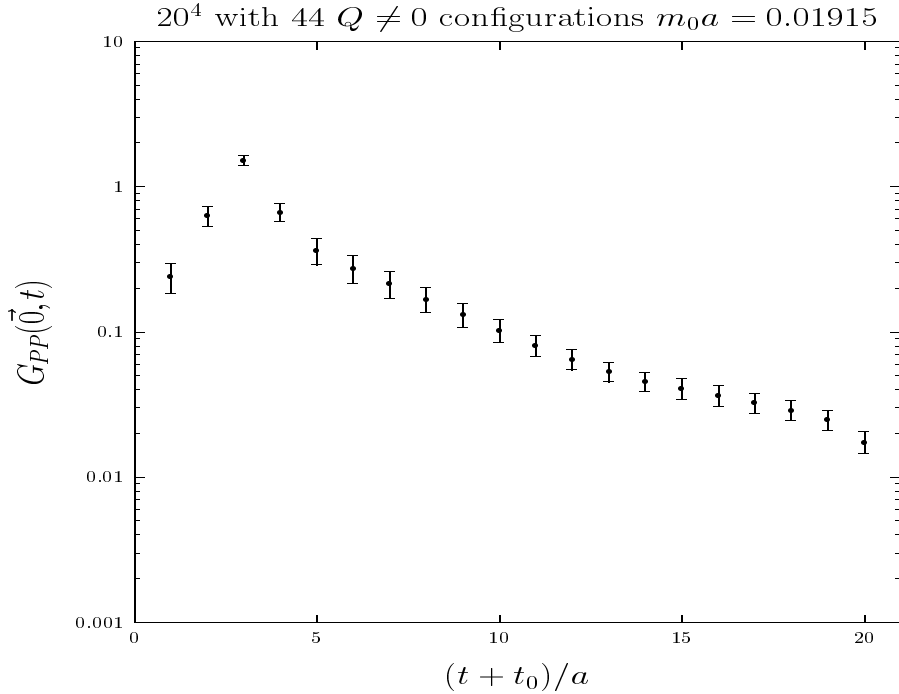


Figure 4: The same as in Fig. 3 for 44 configurations with $Q \neq 0$.

Comparing with the generalized GOR relation in Eq. (5), we see the first term corresponds to $\frac{\langle Q \rangle}{m_0 V}$ term in Eq. (4) and the second term vanishes due to the orthogonality between the zero modes and the non-zero modes. In either case, we expect that the number of zero modes grows with \sqrt{V} and the eigenfunction $\psi(0) \propto 1/\sqrt{V}$. As a result, both zero-mode terms in Eqs. (7) and (8) decrease with volume like $1/\sqrt{V}$ and are finite volume artifacts.

The most straight-forward way of isolating the zero mode contribution is to calculate their eigenvectors and project them out as is done in Ref. [26]. However, this is very costly, as costly as calculating the quark propagator itself.

We show the pseudoscalar propagator for a light quark mass ($m_0 a = 0.01915$) in Fig. 2 and we see that there appears a kink at $t/a \sim 8 - 9$ (The source is placed at $t_0/a = 3$ so that it appears at $(t + t_0)/a \sim 11 - 12$.) To further explore its origin, we separate the 63 configurations into 19 with trivial topology (i.e. $Q = 0$) and 44 with non-trivial topology (i.e. $Q \neq 0$) and plot the respective pseudoscalar propagators in Figs. 3 and 4.

We see that the propagator on the $Q = 0$ configurations (Fig. 3) has a single exponential all the way from $t/a = 5$ to 14. Upon fitting a single exponential in this range, we find $m_{Pa} = 0.153(12)$. On the other hand, the propagator of the $Q \neq 0$ configurations (Fig. 4) still has a pronounced kink at $t/a \sim 8$. When we fit it in the range $t/a = 8 - 14$, the mass is $m_{Pa} = 0.146(32)$ which is quite consistent with that from the $Q = 0$ configurations. On the other hand, when we fit the time range t/a from 4 to 8, $m_{Pa} = 0.245(58)$ which is quite a bit higher than that of the $Q = 0$

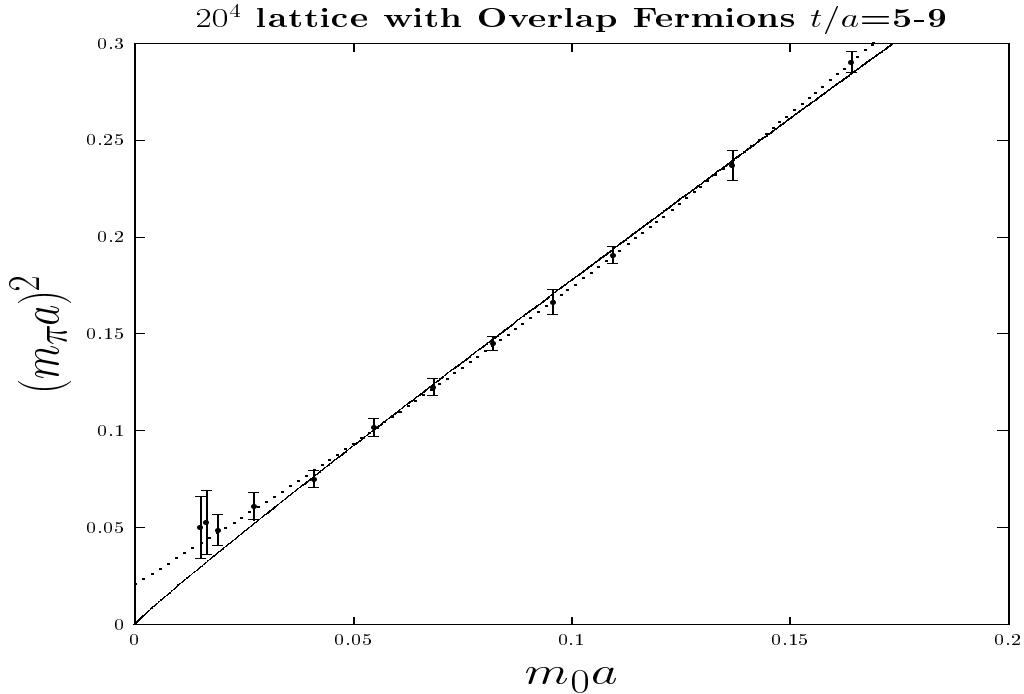


Figure 5: $m_P^2 a^2$ vs $m_0 a$ with a fit of $m_P a$ in the window of $t/a = 5 - 9$. The dotted line is a fit linear and quadratic in $m_0 a$. The solid line is a fit including the chiral log.

configurations. We take this as the evidence that the zero-mode contributions, the combined direct and cross terms, fall off faster in t/a than the pseudoscalar mass. We can thus use the time separation as the filter to obtain the masses and decay constants of the physical pseudoscalar mesons. Now we can understand why in the previous studies of m_P , the m_P^2 does not approach zero with the quark mass [24, 25]. In Ref. [24], the lattice size is $6^3 \times 12$ with $\beta = 5.7$. Since it uses the fixed boundary condition in the time direction, the maximum usable time separation is about 7. This translates into time separation of ~ 9 on our lattice. In Ref. [25], the lattice size is $12^3 \times 24$ with $\beta = 5.9$. In this study, the authors use the periodic boundary condition in time, time slices up to 12 are fitted which corresponds to ~ 10 on our lattice. In either case, the fitted time range is expected to be contaminated by the zero mode contribution and result in a higher mass for a given quark mass. To verify this, we fit our data in the time range $t/a = 5 - 9$ and plot the resulting $m_P^2 a^2$ in Fig. 5. We see that they indeed don't approach zero with a fit linear and quadratic in $m_0 a$ (dashed line), similar to those shown in Refs. [24, 25]. One may attempt to interpret the data to include a chiral log and force the pion mass to go to zero in the chiral limit. This can be misleading. We shall defer the discussion of the complication due to the quenched chiral log in Sec. 5.

In principle, one can overcome the zero mode problem by fitting the zero momentum pion propagator $G_{PP}(\vec{p} = 0, t)$ in a time range beyond the localized zero mode contribution, such as beyond $(t + t_0)/a > 12$ in Fig. 2. Unfortunately, our data at larger time slices are tainted by the reflection from the fixed boundary at

$(t + t_0)/a = 20$ when the quark mass is small so that the fit in the limited time window to avoid both the zero mode and the boundary reflection is unsettling in this case. For this reason, we examine the propagator $G_{A_4P}(\vec{p} = 0, t)$ instead. Since the zero modes on one gauge configuration have the same chirality, the pure zero mode contribution (i.e. the direct zero mode contribution which corresponds to the first term on the right-hand-side of Eq. (7)) vanishes. The cross-term between the zero modes and the non-zero modes does not vanish, but is expected to be small due to cancellations. We plot in Fig. 6 $G_{A_4P}(\vec{p} = 0, t)$ for the same quark mass $m_0a = 0.01915$ and we do not see a kink in the range $5 < (t + t_0)/a < 15$ as is in $G_{PP}(\vec{p} = 0, t)$ in Fig. 2. Thus, we shall calculate the pseudoscalar masses from $G_{A_4P}(\vec{p} = 0, t)$. The results of $m_P^2 a^2$ so obtained are plotted in Fig. 7.

Comparing with Fig. 5, we note that $m_P^2 a^2$ in Fig. 7 which are free from the zero mode contamination are lower than the corresponding ones in Fig. 5 for small quark masses. How $m_P^2 a^2$ approaches zero in the chiral limit is complicated by the presence of the quenched chiral log. We shall postpone this discussion until Sec. 5, except to mention that the solid line in Fig. 7 is the fit with the chiral log and the dashed line is the fit with linear and quadratic terms in m_0a .

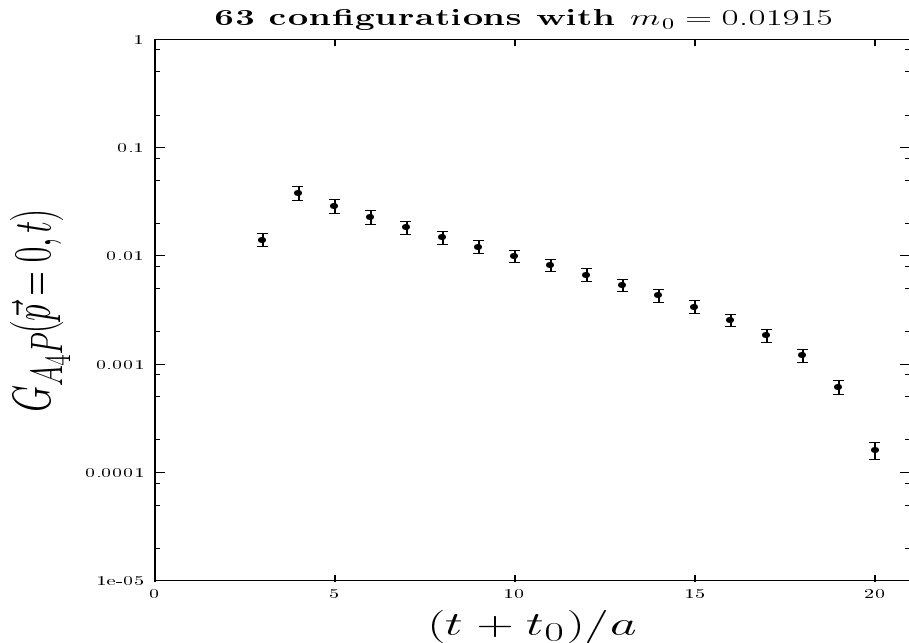


Figure 6: Propagator $G_{A_4P}(\vec{p} = 0, t)$ for $m_0a = 0.01915$ for all 63 configurations.

The zero mode contributions to mesons can be written as

$$\int d^3x \langle M(x)M(0) \rangle|_{zero\ modes} = \tag{9}$$

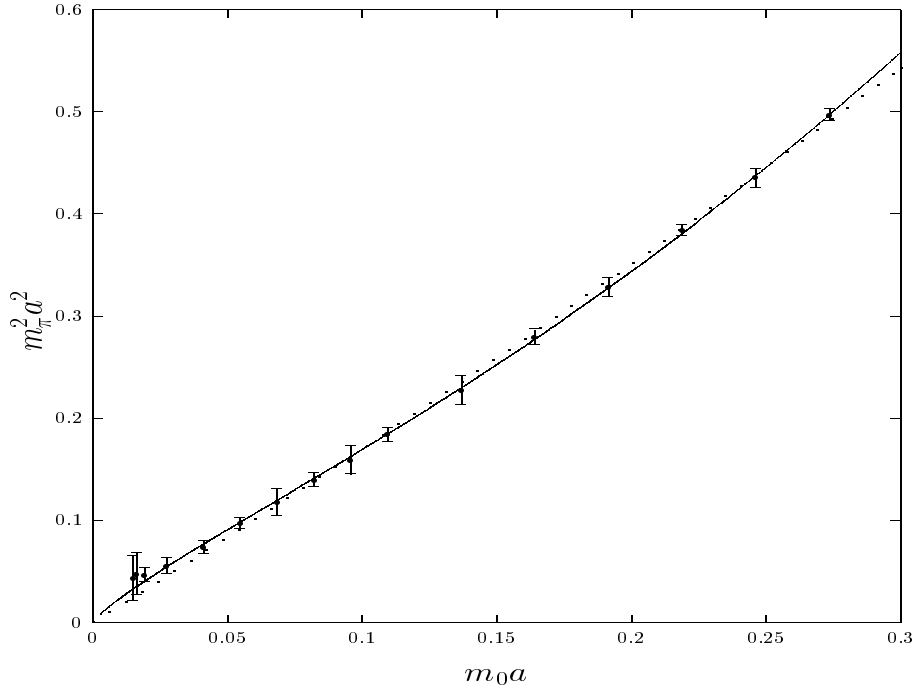


Figure 7: $m_p^2 a^2$ vs $m_0 a$ calculated from $G_{A_4 P}(\vec{p} = 0, t)$. The linear plus quadratic fit (dotted line) and the chiral log fit (solid line) from Eq. (32) with $\Lambda_\chi = 0.8$ GeV are discussed in Sec. 5.

$$\begin{aligned}
& - \int d^3 x \left[\sum_{i,j=\text{zeromodes}} \frac{\text{tr}(\psi_j^\dagger(x) \gamma_5 \Gamma \psi_i(x)) \text{tr}(\psi_i^\dagger(0) \bar{\Gamma} \gamma_5 \psi_j(0))}{m_0^2} \right. \\
& \left. + 2 \sum_{i=0, \lambda > 0} \frac{\text{tr}(\psi_\lambda^\dagger(x) \gamma_5 \Gamma \psi_i(x)) \text{tr}(\psi_i^\dagger(0) \bar{\Gamma} \gamma_5 \psi_\lambda(0))}{m_0(\lambda^2 + m_0^2)} \right], \quad (10)
\end{aligned}$$

where Γ and $\bar{\Gamma}$ are the gamma matrices for the corresponding meson interpolation fields. For the pseudoscalar meson as we discussed above, $\Gamma = -\bar{\Gamma} = \gamma_5$. For the scalar meson (the connected insertion part), $\Gamma = \bar{\Gamma} = 1$. Since the zero modes are the eigenstates of γ_5 , i.e. $\gamma_5 \psi_{i=0} = \pm \psi_{i=0}$, the zero mode contribution in the scalar propagator has a negative sign from that in the pseudoscalar propagator. Thus, it is suggested [23, 6, 7] to consider $\int d^3 x [\langle \pi(x) \pi(0) \rangle + \langle \sigma(x) \sigma(0) \rangle]$ where the zero-mode contributions cancel and at large t/a it should be dominated by the pseudoscalar. However, there is a problem. As will be shown in a separate publication [27], the large time part of the isovector-scalar propagator for the quark mass range that we are concerned turns out to be negative. It is pointed out in a study with pole-shifting in the Wilson action [28] that it is dominated by the would-be η' and π intermediate state which is negative due to quenching. In the intermediate time region, there is still the contribution from η' and π intermediate state besides the a_0 . As a consequence, the addition of the pseudoscalar and scalar meson is not a viable solution to obtaining the pseudoscalar mass. It is also suggested that the axial-vector interpolation field with $\Gamma = \bar{\Gamma} = \gamma_4 \gamma_5$ does not have the direct term contribution from the zero modes since all the zero modes have the same chirality in a given gauge configuration. However, the second term in Eq. (9) may still have a contribution. Since it is a cross term, it might

be small due to cancellations. Unfortunately, our data on the $\langle A_4 A_4 \rangle$ correlator are much noisier than the $\langle \pi \pi \rangle$ correlator, since $\langle 0 | A_4 | \pi(0) \rangle = \sqrt{2} m_\pi f_\pi$ which diminishes when the pion mass is small. We cannot conclude anything from them.

It appears that, short of projecting out the zero modes from the meson propagators, fitting the pseudoscalar mass from the propagator $G_{A_4 P}(\vec{p} = 0, t)$ is probably the only practical way of getting reasonably reliable and accurate pseudoscalar masses for our lattice with fixed boundary condition.

4 Z_A and Pion Decay Constant f_π

It has been pointed out in our earlier work [8] that the renormalization constant Z_A for the axial current $A_\mu = \bar{\psi}(i\gamma_\mu \gamma_5(1 - D/2\rho)\frac{\tau^a}{2})\psi$ can be obtained directly through the axial Ward identity

$$Z_A \partial_\mu A_\mu = 2Z_m m_0 Z_P P, \quad (11)$$

where $P = \bar{\psi}(i\gamma_5(1 - D/2\rho)\frac{\tau^a}{2})\psi$ is the pseudoscalar density. Since $Z_m = Z_S^{-1}$ and $Z_S = Z_P$ due to the fact that the scalar density $\bar{\psi}(1 - D/2\rho)\frac{\tau^a}{2}\psi$ and the pseudoscalar density P are in the same chiral multiplet, Z_m and Z_P cancel in Eq. (11) and one can determine Z_A to $O(a^2)$ non-perturbatively from the axial Ward identity using the bare mass m_0 and bare operator P . To obtain Z_A , we shall consider the on-shell matrix elements between the vacuum and the zero-momentum pion state for the axial Ward identity

$$Z_A \langle 0 | \partial_\mu A_\mu | \pi(\vec{p} = 0) \rangle = 2m_0 \langle 0 | P | \pi(\vec{p} = 0) \rangle, \quad (12)$$

where the matrix elements can be obtained from the zero-momentum correlators

$$\begin{aligned} G_{\partial_4 A_4 P}(\vec{p} = 0, t) &= \langle \sum_{\vec{x}} \partial_4 A_4(x) P(0) \rangle \\ G_{PP}(\vec{p} = 0, t) &= \langle \sum_{\vec{x}} P(x) P(0) \rangle. \end{aligned} \quad (13)$$

The non-perturbative Z_A is then

$$Z_A = \lim_{t \rightarrow \infty} \frac{2m_0 G_{PP}(\vec{p} = 0, t)}{G_{\partial_4 A_4 P}(\vec{p} = 0, t)}. \quad (14)$$

There has been extensive study [29, 30, 31, 32] of the $O(a)$ improvement of the Wilson action and composite operators in relation to the chiral symmetry and axial Ward identity. It has been shown [30] that in the improved mass-independent renormalization scheme, the renormalized improved axial current and pseudoscalar density have the following form from an $O(a)$ improved action

$$\begin{aligned} A_\mu^R &= Z_A(1 + b_A m_q a) \{A_\mu + c_A a \partial_\mu P\}, \\ P^R &= Z_P(1 + b_P m_q a) P, \end{aligned} \quad (15)$$

20⁴ Lattice with Overlap Fermions

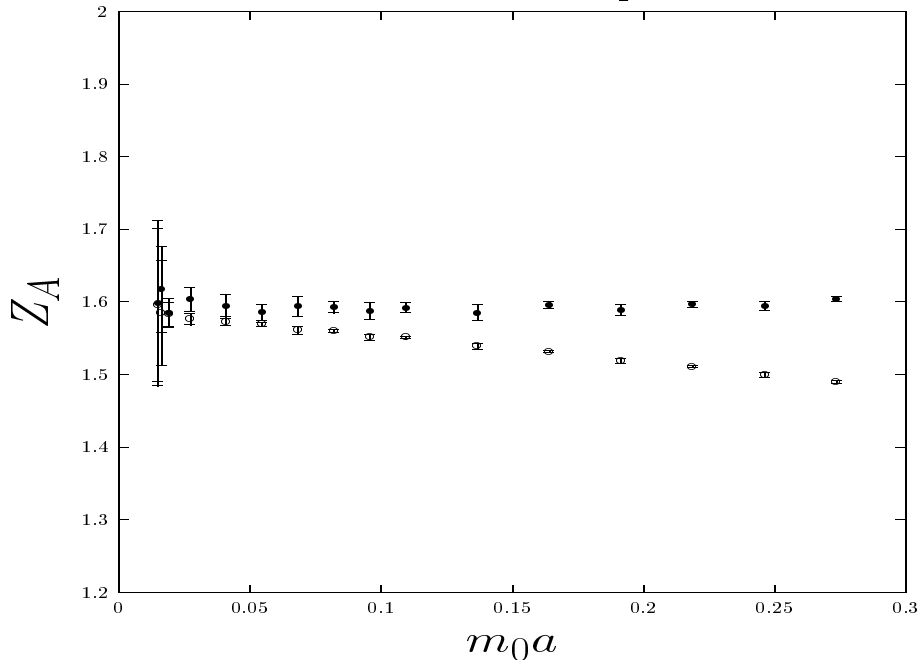


Figure 8: Z_A vs quark mass $m_0 a$. The results from Eq. (14) are indicated by \circ and those from Eq. (17) are indicated by \bullet .

where $m_q = m_0 - m_c$ is the subtracted quark mass and c_A, b_A and b_P are improvement coefficients. The renormalization constants Z_A and Z_P are functions of the modified coupling $\tilde{g}_0^2 = g_0^2(1 + b_g m_q a)$. Now that the overlap fermion is $O(a)$ improved [33], it satisfies the Ginsparg-Wilson relation [34] and the quark mass is not additively renormalized. As a result, $b_A = c_A = b_P = 0$. The renormalization constant Z_A determined from Eq. (14) has only $O(a^2)$ error as a consequence. Z_A thus computed for all the quark masses are plotted in Fig. 8 as indicated by the open circles. We see that there is still an appreciable $O(a^2)$ error. Given that the time derivative itself in $G_{\partial_4 A_4 P}(\vec{p} = 0, t)$ invokes an $O(a^2)$ error, it would be better to adopt a definition for Z_A which is devoid of this superfluous $O(a^2)$ error. This can be achieved by noticing that, at large t where the pion state dominates the propagator $G_{\partial_4 A_4 P}(\vec{p} = 0, t)$, one can effectively make the substitution

$$G_{\partial_4 A_4 P}(\vec{p} = 0, t) \xrightarrow{t \rightarrow \infty} m_\pi G_{A_4 P}(\vec{p} = 0, t). \quad (16)$$

Consequently, Eq. (14) becomes

$$Z_A = \lim_{t \rightarrow \infty} \frac{2m_0 G_{PP}(\vec{p} = 0, t)}{m_\pi G_{A_4 P}(\vec{p} = 0, t)}. \quad (17)$$

We plot the results of Z_A from Eq. (17) in Fig. 8. Save for the last two points at the smallest masses ($m_0 a = 0.01505$ and 0.01642), the errors are small. We should point out that it is conspicuously flat as a function of $m_0 a$ indicating that the $O(a^2)$ error from the action and the operators is small. We fit them in the form $Z_A + b m_0^2 a^2$ and found that $Z_A = 1.589(4), b = 0.175(73)$ with $\chi^2/DF = 0.30$. We see that Z_A

Table 2: Renormalization constant Z_A from Eq. (14) (column 2), and Eq. (17) (column 3).

m_0a	Z_A (Eq. (14))	Z_A (Eq. (17))
0.2736	1.490(2)	1.605(4)
0.2462	1.499(3)	1.594(6)
0.2189	1.511(2)	1.597(4)
0.1915	1.519(3)	1.589(8)
0.1642	1.532(2)	1.596(5)
0.1368	1.539(4)	1.585(11)
0.1094	1.551(2)	1.592(8)
0.09576	1.552(4)	1.587(12)
0.08208	1.560(2)	1.593(8)
0.06840	1.561(5)	1.594(13)
0.05472	1.569(3)	1.586(12)
0.04104	1.572(5)	1.595(15)
0.02736	1.576(8)	1.604(17)
0.01915	1.583(17)	1.585(20)
0.01642	1.585(72)	1.618(60)
0.01505	1.596(105)	1.598(114)

is determined to the precision of a fraction of 1%. We find it to be larger than the perturbative calculation [12] which gives $Z_A(\mu = 1/a) = 1.213$ for Wilson gauge action with $\beta = 5.85$ which has about the same string tension as our gauge configurations. Z_A from both Eqs. (14) and (17) are tabulated in Table 2.

For the pion decay constant, one can look at the ratio of the zero-momentum correlator

$$G_{A_4P}(\vec{p} = 0, t) = \langle \sum_{\vec{x}} A_4(x) P(0) \rangle, \quad (18)$$

and $G_{PP}(\vec{p} = 0, t)$,

$$f_\pi a = \lim_{t \rightarrow \infty} \frac{Z_A G_{A_4P}(\vec{p} = 0, t)}{\sqrt{m_\pi a} G_{PP}(\vec{p} = 0, t)} e^{m_\pi t/2}. \quad (19)$$

For our definition of the isovector axial and pseudoscalar currents, the experimental f_π is 92.4 MeV.

Combining with Z_A from Eq. (14), we obtain

$$f_\pi a = \lim_{t \rightarrow \infty} \frac{2m_0a \sqrt{G_{PP}(\vec{p} = 0, t)} G_{A_4P}(\vec{p} = 0, t)}{\sqrt{m_\pi a} G_{\partial_t A_4P}(\vec{p} = 0, t)} e^{m_\pi t/2}. \quad (20)$$

We first fit the pion masses from $G_{A_4P}(\vec{p}=0, t)$ and feed them into Eq. (20). Unlike the case with Z_A in Eqs. (14) and (17) where the boundary effects on the common source for the interpolation field P in the numerator and denominator cancel, they don't cancel in f_π . To correct for this, we replace $\sqrt{G_{PP}(\vec{p}=0, t)}$ with $G_{PP}(\vec{p}=0, t) e^{m_\pi t/2} / \sqrt{G_{PP}(\vec{p}=0, (N_t+1)a - t_0) e^{m_\pi((N_t+1)a - t_0)}}$ which should get rid of the boundary effect which affects the matrix element $\langle 0|P|\pi\rangle$ associated with the source in G_{PP} . The errors of the ratio are obtained with the jackknife method. We plot the result in Fig. 9 as a function of m_0a as open circles. We also tabulate them in Table 3 together with the pion mass computed from $G_{A_4P}(\vec{p}=0, t)$.

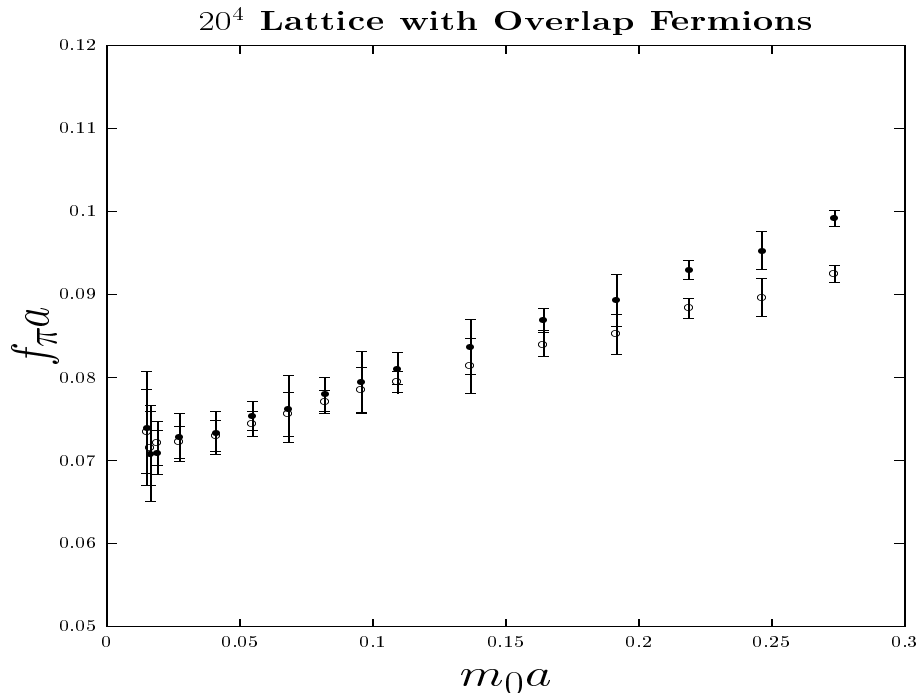


Figure 9: Renormalized $f_\pi a$ vs quark mass $m_0 a$.

As in the case of Z_A defined from $G_{\partial_4 A_4 P}(\vec{p}=0, t)$, f_π defined from Eq. (20) contains $O(a^2)$ error invoked by the time derivative. We shall again make the substitution in Eq. (16) and arrive at

$$f_\pi a = \lim_{t \rightarrow \infty} \frac{2m_0 a \sqrt{G_{PP}(\vec{p}=0, t)} m_\pi a e^{m_\pi t/2}}{(m_\pi a)^2}. \quad (21)$$

The results are listed in Table 3 and plotted in Fig. 9 as \bullet . The difference from the \circ reflects the $O(a^2)$ error due to the time derivative in $G_{\partial_4 A_4 P}(\vec{p}=0, t)$. With all

16 data points in a linear fit, we find

$$f_\pi a = 0.0691(11) + 0.109(56) m_0 a, \quad (22)$$

with $\chi^2/DF = 0.03$. We note that it yields an error of only 1.6% in the chiral limit. Given that it is a physical observable from the fermion operator without the chiral log in a quenched theory [35] and with such high precision, it is an ideal quantity to set the scale of the lattice. Comparing with the experimental value $f_\pi = 92.4$ MeV, we determine the scale of our lattice to be $a = 0.148(2)$ fm. This is about 14% higher than that determined from the string tension with $\sqrt{\sigma} = 440$ MeV and 20% larger than that determined from r_0 . This is quite consistent with other quenched calculations.

Our results on f_π and its quark mass dependence are consistent with those calculated with the domain-wall fermion [23] and the overlap fermion [7] on smaller lattices and higher pion masses.

Table 3: Pion masses obtained from $G_{A_4P}(\vec{p} = 0, t)$ are listed together with $f_\pi a$ from Eq. (20) (column 4), and Eq. (21) (column 5), and $f_P a^2$ from Eq. (34).

$m_0 a$	$m_\pi a$	$m_\pi^2 a^2$	$f_\pi a$ (Eq. (20))	$f_\pi a$ (Eq. (21))	$f_P a^2$
0.2736	0.705(4)	0.497(6)	0.0925(10)	0.0991(10)	0.1273(13)
0.2462	0.660(7)	0.436(9)	0.0896(23)	0.0952(23)	0.1192(28)
0.2189	0.620(4)	0.384(5)	0.0883(12)	0.0929(11)	0.1155(14)
0.1915	0.573(8)	0.328(9)	0.0852(24)	0.0893(31)	0.1082(38)
0.1642	0.529(7)	0.280(7)	0.0839(14)	0.0869(13)	0.1048(16)
0.1368	0.477(15)	0.228(14)	0.0813(33)	0.0837(33)	0.0983(39)
0.1094	0.429(8)	0.184(7)	0.0794(13)	0.0810(19)	0.0963(22)
0.09576	0.399(17)	0.159(14)	0.0784(28)	0.0794(37)	0.0934(43)
0.08208	0.374(9)	0.140(7)	0.0770(13)	0.0779(21)	0.0939(25)
0.06840	0.343(19)	0.118(13)	0.0755(26)	0.0762(40)	0.0927(49)
0.05472	0.312(9)	0.0973(56)	0.0744(15)	0.0753(18)	0.0942(30)
0.04104	0.272(12)	0.0740(65)	0.0729(18)	0.0733(25)	0.0933(32)
0.02736	0.236(17)	0.0557(80)	0.0722(19)	0.0728(29)	0.1055(34)
0.01915	0.216(16)	0.0467(69)	0.0721(26)	0.0709(27)	0.1222(42)
0.01642	0.218(47)	0.0475(205)	0.0714(44)	0.0708(58)	0.145(12)
0.01505	0.209(53)	0.0437(221)	0.0734(50)	0.0738(68)	0.152(14)

5 Quenched Chiral Logs

In the quenched approximation of QCD, one ignores the virtual quark loops. One of the consequences is that the flavor-singlet meson propagator (which we shall refer to as η' even though the physical η' is not completely flavor-singlet and has octet mixture) has a double pole in the Veneziano model for the U(1) anomaly [36, 37]. As such, it does not move the mass of the would-be Goldstone boson to the large η' mass. Consequently, this leads to infrared singular η' loops with the hair-pin type diagrams in the renormalization of hadron masses and certain matrix elements and thus alters their chiral behaviors from those of full QCD with dynamical fermions.

The first study of the anomalous chiral behavior was done by Sharpe [35] and Bernard and Golterman [38] in quenched chiral perturbation theory. They predicted the chiral-log pathologies in the pseudoscalar meson masses, $\langle\bar{\psi}\psi\rangle$, the f_K/f_π ratio, etc. The first evidence of the chiral-log was observed by the CP-PACS Collaboration [39] in the ratio of pseudoscalar meson masses with two unequal quark masses with the Wilson fermion. They obtain the chiral log parameter $\delta = 0.8 - 1.2$. A more extensive study [40] which invokes the shifting of the real poles of the quark propagator to improve the otherwise poor chiral properties of the Wilson fermion near the chiral limit was carried out to examine the quenched chiral logs in the pseudoscalar masses and the pseudoscalar decay constants, obtaining consistent results with $\delta = 0.065 \pm 0.013$. The same quenched chiral log is also observed in the ratio of m_π^2/m_q with the Kogut-Susskind action [41] with $\delta = 0.061 \pm 0.03$. All of them are small compared to that expected from the coupling of the would-be Goldstone bosons (or quark loops in the pseudoscalar channel) which is responsible for the η' mass of the U(1) anomaly. Recently, the small nonzero eigenvalues of the Overlap Dirac operator were calculated in a deconfined phase [42] and it was found that the chiral condensate diverges at the infinite volume limit indicating a quenched singularity consistent with the quenched chiral perturbation prediction $\langle\bar{\psi}\psi\rangle \propto m^{-\frac{\delta}{1+\delta}}$.

Given that the overlap fermion has the promise of exact chiral symmetry on the lattice, it is natural to look for these chiral singularities and check if the quenched chiral logs seen in the Wilson and Kogut-Susskind fermions can be verified with the overlap action. The first attempt to extract the chiral log from the pion mass on several small volumes was inconclusive [8]. We shall examine them here on a much larger volume.

The behavior of the quenched chiral logs can be seen from the sigma model [40] with $U(3) \times U(3)$ where the pseudoscalar field is represented by

$$U = e^{\phi_0/f} e^{i \sum_{a=1}^8 \lambda_a \phi_a/f}, \quad (23)$$

where λ_a is the SU(3) flavor matrix and ϕ_a are the octet Goldstone boson fields. The U(1) part is described by η' field with $\phi_0 = \sqrt{2/N_f} \eta'/f$ where N_f is the number of

flavors which is 3 in our case. The effect of the chiral logs can be understood as the renormalization effect of integrating out the η' [40]. The resulting $SU(3) \times SU(3)$ will be represented by the renormalized U

$$U = e^{-\langle\phi_0^2\rangle/2f^2} e^{\sum_{a=1}^8 \lambda_a \phi_a/f}. \quad (24)$$

In the quenched approximation, the integral representing the η' loop involves only the hair-pin diagram of two would-be singlet Goldstone boson (we shall refer to it as η and it has the same mass as π) propagators

$$\langle\phi_0^2\rangle = \frac{2}{VN_f} \int d^4x \langle\eta(x)\eta(x)\rangle = \int \frac{d^4p}{(2\pi)^4 N_f} \frac{-\bar{m}_0^2}{p^2 + m_\pi^2} = \frac{-\bar{m}_0^2}{16\pi^2 N_f} (\ln \frac{\lambda^2}{m_\pi^2} - 1) \quad (25)$$

Therefore, the infrared singular part of U in Eq. (24) can be represented by δ

$$U = e^{-\delta \ln m_\pi^2} e^{\sum_{a=1}^8 \lambda_a \phi_a/f} = \left(\frac{1}{m_\pi^2}\right)^\delta e^{\sum_{a=1}^8 \lambda_a \phi_a/f}, \quad (26)$$

where

$$\delta = \frac{\bar{m}_0^2}{16\pi^2 N_f f^2}. \quad (27)$$

From the Witten-Veneziano model of the η' mass, $\bar{m}_0 \sim 870\text{MeV}$. This gives an estimate of $\delta = 0.183$.

To see the effects on various physical quantities, one can first look at pseudoscalar density and axial current operators [40]. In the sigma model,

$$\begin{aligned} \bar{\psi} i \gamma_5 \psi &\propto U - U^\dagger \\ \bar{\psi} i \gamma_\mu \gamma_5 \psi &\propto i[U^{-1} \partial_\mu U - (\partial_\mu U^{-1}) U]. \end{aligned} \quad (28)$$

With U given in Eq. (26), one arrives at

$$\begin{aligned} f_P &= \langle 0 | \bar{\psi} i \gamma_5 \psi | \pi(\vec{p}=0) \rangle = \left(\frac{1}{m_\pi^2}\right)^\delta \tilde{f}_P \\ f_\pi &= \langle 0 | \bar{\psi} i \gamma_\mu \gamma_5 \psi | \pi(\vec{p}=0) \rangle / \sqrt{2} m_\pi = \tilde{f}_\pi \end{aligned} \quad (29)$$

where f_P is the pseudoscalar decay constant and f_π is the axial decay constant and \tilde{f}_P and \tilde{f}_π are constants for small quark masses. Thus, one expects that that f_P is singular as the quark masses approaches zero in the quenched approximation; whereas f_π remains a constant. From the axial Ward identity in Eq. (11) and Eq. (29), one expects

$$m_\pi^2 \propto m_q \frac{f_P}{f_\pi} \propto m_q \left(\frac{1}{m_\pi^2}\right)^\delta, \quad (30)$$

where m_q is the quark mass and therefore

$$m_\pi^2 \propto m_q^{\frac{1}{1+\delta}} \quad (31)$$

which is the behavior predicted in quenched χPT [35].

Given $m_\pi a$ fitted from $G_{A_4 P}(\vec{p} = 0, t)$ and listed in Table 3, we first fit them in the form in Eq. (31) for a range of small quark mass points. We list the fitted δ and χ^2/DF in Table 4. We find that δ ranges from 0.145(66) to 0.24(12). Beyond this range of 8 to 11 smallest quark masses, the errors are greater than half of the fitted δ value.

Table 4: Quenched chiral log parameter δ and χ^2/DF as fitted from $m_\pi^2 a^2$ in Eq. (31).

# of smallest $m_0 a$	δ	χ^2/DF
8	0.24 (12)	0.24
9	0.224(91)	0.22
10	0.163(75)	0.28
11	0.145(66)	0.28

Since the form in Eq. (31) is limited to small $m_0 a$, we shall also fit $m_\pi^2 a^2$ with the form [38, 39]

$$m_\pi^2 a^2 = Am_0 a \{1 - \delta [\ln(Am_0 a / \Lambda_\chi^2 a^2) + 1]\} + Bm_0^2 a^2, \quad (32)$$

which allows a fit to cover the whole range of 16 quark masses. The best fits which give stable values of A and B and with errors less than half of the fitted values of δ for a range of $\Lambda_\chi = 0.6$ GeV to 1.4 GeV are listed in Table 5.

Table 5: Quenched chiral log parameter δ and χ^2/DF as fitted from m_π^2 in Eq. (32).

Λ_χ (GeV)	A	B	δ	χ^2/DF
0.6	1.72(7)	3.0(8)	0.23(7)	0.18
0.8	1.42(11)	3.0(8)	0.28(11)	0.18
1.0	1.17(24)	3.0(8)	0.34(17)	0.18

They are consistent with those fitted in the exponential form, albeit with values of δ between 0.2 and 0.3 which are somewhat higher than those from the exponential form.

We plot the fit with $\Lambda_\chi = 0.8$ GeV as a solid line in Fig. 7. To check if there is indeed a bona fide quenched chiral log, we fit $m_\pi^2 a^2$ alternatively with powers in $m_0 a$

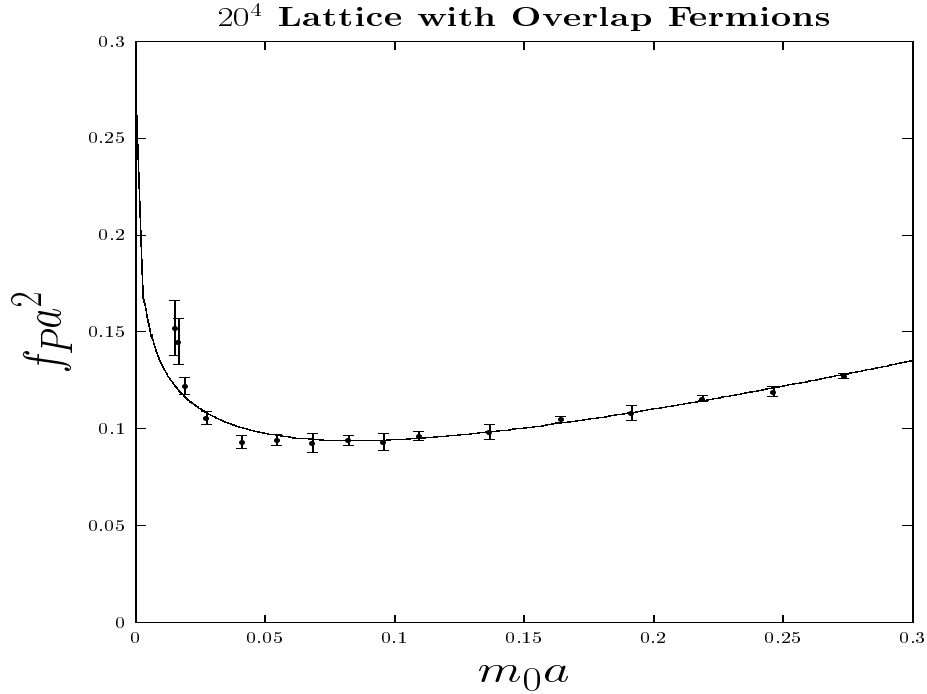


Figure 10: Renormalized $f_P a^2$ vs quark mass $m_0 a$. The solid line is a fit excluding the two smallest quark masses with $\Lambda_\chi = 0.8$ GeV in Eq. (35).

up to cubic terms and found

$$\begin{aligned}
 m_\pi^2 a^2 &= 1.65(5) m_0 a + 0.54(21) m_0^2 a^2, & \chi^2/DF &= 0.90, \\
 m_\pi^2 a^2 &= 1.88(10) m_0 a - 2.3(11) m_0^2 a^2 + 7.8(30) m_0^3 a^3, & \chi^2/DF &= 0.46. \quad (33)
 \end{aligned}$$

The fit including the cubic term in $m_0 a$ is shown in Fig. 7 as the dotted line. We see that in either case, the χ^2/DF is larger than that with the quenched chiral log in Table 5 which is 0.18. From this, we conclude that the quenched chiral is seen in our data for $m_\pi^2 a^2$.

We should point out that if we were to use the $m_P^2 a^2$ data from the shorter time range such as the one with $t/a = 5 - 9$ as plotted in Fig. 5 and insist on fitting them with a power form in Eq. (31), we would find that one can fit the last 12 mass points with $\delta = 0.054 \pm 0.028$ and $\chi^2/DF = 0.98$. This is plotted as the solid line in Fig. 5. This serves as a caveat to show that one can misconstrue the contamination of the zero modes as the quenched chiral log.

Finally, we look for the chiral log in f_P , which according to Eq. (29) should grow in the form of $(\frac{1}{m_\pi^2})^\delta$. We calculate the renormalized f_P from

$$f_P a^2 = \lim_{t/a \gg 1} Z_P \sqrt{G_{PP}(t) 2m_P a e^{m_P t/2}}, \quad (34)$$

where we insert the fitted $m_P a$ to obtain $f_P a^2$. The $\sqrt{G_{PP}(t)}$ is understood to have included the correction of the boundary reflection discussed in Sec. 4 in association

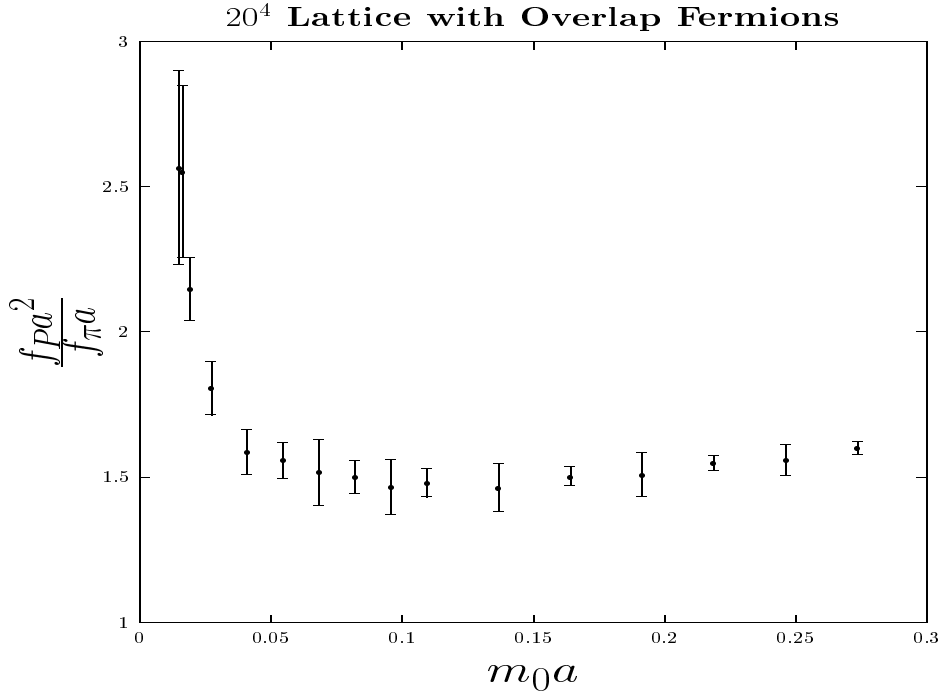


Figure 11: Renormalized $f_P a^2 / f_\pi a$ vs $m_\pi^2 a^2$. The solid line is a fit over the lowest 14 points.

with the determination of f_π . The renormalization constant Z_P is the same as the scalar renormalization constant Z_S . The latter is determined from the matching of renormalization group invariant quark masses at fixed pseudoscalar mass [9] and the details will be given elsewhere [43]. We plot the renormalized $f_P a^2$ in Fig. 10 as a function of $m_0 a$. We see that it rises sharply at small quark mass. Since the log form in Eq. (32) falls off slower at larger quark mass, it gives a more stable fit covering a larger range of the quark mass than the exponential form. Based on this observation, we fit f_P in the log form

$$f_P a^2 = \tilde{f}_P a^2 \{1 - \delta [\ln(A m_0 a / \Lambda_\chi^2 a^2) + 1]\} + B m_0 a, \quad (35)$$

where we input A from the fit to m_P^2 in Eq. (32). It turns out that fits covering the whole range of 16 points have χ^2/DF greater than unity mainly due to the fact the $f_P a^2$ of the two smallest quark masses are too high. Since errors of these two points are large and they are more susceptible to systematic errors from the boundary effect for such low pion masses, we shall ignore them and fit Eq. (35) with the other 14 points. Again, results with reasonably small errors and χ^2/DF less than unity are reported in Table 6.

We see that δ obtained from $f_P a^2$ is consistent with those determined from $m_\pi^2 a^2$. Combining all the fits from $m_\pi^2 a^2$ and $f_P a^2$, δ appears to span the range from 0.15 to 0.4 which is consistent with that predicted from the quenched η' loop in the chiral perturbation theory in Eq. (27) [35, 28], although it tends to be on the high side. We

Table 6: $\tilde{f}_P a^2$, δ and χ^2/DF as fitted for $f_P a^2$ in Eq. (35) are listed.

Λ_χ (GeV)	$\tilde{f}_P a^2$	δ	B	χ^2/DF
0.6	0.083(2)	0.35(4)	0.36(2)	0.93
0.8	0.060(3)	0.48(7)	0.36(2)	0.93

note that the general behavior of our data is close to what are observed in Ref. [28, 41], but our δ is about three to six times larger than theirs.

To alleviate the apprehension that the apparent singular behavior of $f_P a^2$ may be caused by certain unknown boundary effect on the source in our lattice with fixed boundary condition, we consider the ratio of f_P in Eq. (34) and f_π in Eq. (20)

$$f_P a^2 / f_\pi a = \lim_{t \rightarrow \infty} \frac{Z_P \sqrt{2} m_P a G_{\partial_4 A_4 P}(\vec{p} = 0, t)}{2 m_0 a G_{A_4 P}(\vec{p} = 0, t)}. \quad (36)$$

This should cancel out the boundary effect on the source. We plot the ratio $f_P a^2 / f_\pi a$ as a function of $m_\pi^2 a^2$. We see from Fig. 11 that the singular behavior is still visible in $f_P a^2 / f_\pi a$ which confirms that the chiral log singularity is indeed present in f_P .

6 Summary

To conclude, we have studied the chiral properties of the pseudoscalar meson on a quenched lattice with overlap fermions. The lattice size is 20^4 with lattice spacing $a = 0.148$ fm set by the pion decay constant f_π . This gives a physical size of 3.0 fm which is about 4 times the Compton wavelength of the lowest mass pion.

We first clarified the role of the zero modes in the pseudoscalar meson propagator in association with the generalized Gell-Mann-Oakes-Renner relation. We find that the zero mode contribution to the pseudoscalar meson propagators extends to a fairly long distance in the time separation and it is imperative to avoid it since it is a finite volume effect. Otherwise, one might be led to wrong conclusions about the behavior of the pion mass and decay constants near the chiral limit. For example, if one fits the pion mass by choosing a time window which straddles over the kink in Fig. 2, one will find that the pion mass squared does not approach zero at the chiral limit with a linear extrapolation in the quark mass. Interpreting it as due to the quenched chiral log, one may fit it with a chiral log form and obtain a positive δ which can be misleading. In view of the fact that the quenched chiral log fit of $m_\pi^2 a^2$ from data obtained from the shorter time range of $G_{PP}(\vec{p} = 0, t)$ as plotted in Fig. 5 has a much smaller δ than the present study and is consistent with that obtained in Ref. [28], it

would be useful to clarify that the shifted real modes (the ‘would be’ zero modes) in the Wilson action are not responsible for the observed quenched chiral logs in $m_\pi^2 a^2$ and $f_P a^2$ in this case.

Due to the chiral symmetry of the overlap fermion, we obtain the non-perturbative renormalization constant $Z_A = 1.589(4)$ from the axial Ward identity. We find it to be fairly independent of $m_0 a$ which is an indication that the $O(a^2)$ error is small. The renormalized pion decay constant f_π has a positive slope with respect to $m_0 a$. With a small error (1.6%) and devoid of the complication of the quenched chiral log, f_π is an ideal physical observable to set the scale of the lattice.

We studied extensively the issue of quenched chiral log. We have clearly seen the quenched chiral log both in the pseudoscalar meson masses with equal quark masses and their pseudoscalar decay constants. Various fits give δ to be in the range of 0.15 to 0.4 which is in accord with that estimated from the double η propagator approximation of the quenched η' loop which predicts it to be ~ 0.18 .

We finally have a reliable tool in the overlap fermion to study the chiral symmetry properties of hadrons at low energies including the quenched chiral logs. One should go to different lattice spacings to study the continuum limit in the future.

This work is partially supported by DOE Grants DE-FG05-84ER40154 and DE-FG02-95ER40907. We wish to acknowledge enlightening discussions and exchanges with L. Giusti, M. Golterman, P. Hernandez, K. Jansen, D. Lin, M. Lüscher, R. Sommer, A. Soni, and C. Rebbi.

References

- [1] For reviews, see for example, H. Neuberger, Nucl. Phys. **B (Proc. Suppl.)** **83-84**, 67 (2000); F. Niedermayer, Nucl. Phys. **B** **73**(Proc. Suppl.), 105 (1999).
- [2] H. Neuberger, Phys. Lett. **B** **417**, 141 (1998).
- [3] R. Narayanan and H. Neuberger, Nucl. Phys. **B** **443**, 305 (1995).
- [4] R.G. Edwards, U.M. Heller and R. Narayanan, Phys. Rev. **D** **59**, 094510 (1999).
- [5] P. Hernández, K. Jansen, and L. Lellouch, Phys. Lett. **B****469**, 198 (1999), [hep-lat/9907022].
- [6] T. DeGrand, hep-lat/0107014.
- [7] L. Giusti, C. Hoelbling, and C. Rebbi, hep-lat/0108007.
- [8] S.J. Dong, F.X. Lee, K.F. Liu, and J.B. Zhang, Phys. Rev. Lett. **85**, 5051 (2000), [hep-lat/0006004].

- [9] P. Hernandez, K. Jansen, L. Lellouch, and H. Wittig, hep-lat/0106011.
- [10] T. Degrand, hep-lat/0106001.
- [11] R.G. Edwards and U.M. Heller, Nucl. Phys. **94 (Proc. Suppl.)**, 737 (2001), [hep-lat/0010035].
- [12] C. Alexandrou, E. Follana, H. Panagopoulos, E. Vicari, Nucl. Phys. **B580**, 394 (2000), [hep-lat/0002010].
- [13] S. Capitani, Nucl.Phys. **B592**, 18 (2001), [hep-lat/0005008].
- [14] R.G. Edwards, U.M. Heller and R. Narayanan, Nucl. Phys. **B540**, 457 (1999).
- [15] R.G. Edwards, U.M. Heller and R. Narayanan, Phys. Rev. **D60**, 034502 (1999).
- [16] M. Lüscher and P. Weisz, Phys. Lett. **B 158**, 250 (1985); M. Alford, W. Dimm, and P. Lepage, Phys. Lett. **B 361**, 87 (1995).
- [17] C.J. Morningstar and M. Peardon, Phys. Rev. **D56**, 4043 (1997).
- [18] P. Hasenfratz, V. Laliena, and F. Niedermayer, Phys. Lett. **B427**, 125 (1998).
- [19] M. Lüscher, Phys. Lett. **B428**, 342 (1998), [hep-lat/9802011].
- [20] P. Chen et al., Nucl. Phys. **B (Proc. Suppl.) 73**, 207 (1999).
- [21] K.F. Liu, S.J. Dong, F.X. Lee, and J.B. Zhang, Nucl. Phys. **B (Proc. Suppl.) 83-84**, 636 (2000).
- [22] H. Leutwyler and A. Smilga, Phys. Rev. **D46**, 5607 (1992).
- [23] T. Blum et al., hep-lat/0007038.
- [24] K.F. Liu, S.J. Dong, F.X. Lee, and J.B. Zhang, Nucl. Phys. **B (Proc. Suppl.) 94**, 752 (2001), [hep-lat/0011072].
- [25] T. DeGrand, A. Hasenfratz, Phys. Rev. **D 64**, 034512 (2001), [hep-lat/0012021].
- [26] R. V. Gavai, S. Gupta, R. Lacaze, hep-lat/0107022.
- [27] S.J. Dong, T. Draper, F.X. Lee, K.F. Liu, and J.B. Zhang, under preparation.
- [28] W. Bardeen, A. Duncan, E. Eichten, N. Isgur, and H. Thacker, hep-lat/0106008.
- [29] G. Heatlie, G. Martinelli, C. Pittori, G.C. Rossi, and C.T. Sachrajda, Nucl. Phys. **B 352**, 266 (1991).
- [30] M. Lüscher, S. Sint, R. Sommer, and P. Weisz, Nucl. Phys. **B 478**, 365 (1996).

- [31] M. Lüscher and P. Weisz, Nucl. Phys. **B 479**, 429 (1996).
- [32] M. Lüscher, S. Sint, R. Sommer, and H. Wittig, Nucl. Phys. **B 491**, 344 (1997).
- [33] Y. Kikukawa, R. Narayanan, and H. Neuberger, Phys. Lett. **B 399**, 105 (1997).
- [34] H. Neuberger, Phys. Lett. **B 427**, 353 (1998).
- [35] S.R. Sharpe, Phys. Rev. **D 46**, 3146 (1992).
- [36] G. Veneziano, Nucl. Phys. **B159**, 213 (1979).
- [37] K.F. Liu, Phys. Lett. **B281**, 141 (1992).
- [38] C.W. Bernard and M. Golterman, Phys. Rev. **D 46**, 853 (1992).
- [39] S. Aoki, et al., Phys. Rev. Lett. **84**, 238 (2000).
- [40] W. Bardeen, A. Duncan, E. Eichten, and H. Thacker, Phys. Rev. **D 62**, 114505 (2000).
- [41] C. Bernard, et al., Phys. Rev. **D64**, 054506 (2001).
- [42] J. Kiskis and R. Narayanan, hep-lat/0106018.
- [43] S.J. Dong, T. Draper, I. Horváth, F.X. Lee, K.F. Liu, and J.B. Zhang, under preparation.